Internal structure and remodeling in dystrophin-deficient cardiomyocytes using second harmonic generation

Béla Varga, Albano C Meli, Silviya Radoslavova, Mathieu Panel, Alain Lacampagne, Csilla Gergely, Olivier Cazorla, Thierry Cloitre

Internal structure and remodeling in dystrophin-deficient cardiomyocytes using second harmonic generation”

Béla Varga, PhD[a,1], Albano C. Meli, PhD[b,1], Silviya Radoslavova, Master degree[a,b], Mathieu Panel, PhD[b], Alain Lacampagne, PhD[b], Csilla Gergely, PhD[a], Olivier Cazorla, PhD[b,*,2], Thierry Cloitre, PhD[a,**,2]

[a]*L2C, University of Montpellier, CNRS, Montpellier, France*
[b]*PhyMedExp, University of Montpellier, CNRS, INSERM, Montpellier, France*

Abstract

Duchenne muscular dystrophy (DMD) is a debilitating disorder related to dystrophin encoding gene mutations, often associated with dilated cardiomyopathy. However, it is still unclear how dystrophin deficiency affects cardiac sarcomere remodeling and contractile dysfunction. We employed second harmonic generation (SHG) microscopy, a nonlinear optical imaging technique that allows studying contractile apparatus organization without histologic fixation and immunostaining. Images were acquired on alive DMD (*mdx)* and wild type cardiomyocytes at different ages and at various external calcium concentrations. An automated image processing was developed to identify individual myofibrils and extract data about their organization. We observed a structural aging-dependent remodeling in *mdx* cardiomyocytes affecting sarcomere sinuosity, orientation and length that could not be anticipated from standard optical imaging. These results revealed for the first time the interest of SHG to evaluate the intracellular and sarcomeric remodeling of DMD cardiac tissue in an age-dependent manner that could participate in progressive contractile dysfunction.

Key words: Second harmonic generation; Sarcomeres; Dystrophin; Cardiomyocytes; Duchenne muscular dystrophy

Introduction

Duchenne muscular dystrophy (DMD) is the worst muscular dystrophy, with an incidence of one in 3500 boys at birth. It affects muscle cell integrity leading to progressive degradation of muscle function with no current therapy available. DMD is associated to mutations silencing the gene encoding dystrophin. Dystrophin acts as a sub-sarcolemmal protein linking the contractile units, namely the sarcomeres, with the extracellular matrix. DMD mutations causing loss-of-function of dystrophin lead to membrane integrity failure, which affects myofiber architecture and has deleterious consequences on the molecular motors and the sarcomeres. Structural changes of the sarcomeres contained in DMD skeletal muscle biopsies have been reported to be linked with muscle weakness and atrophy [1,2]. Ultrastructure analysis of DMD skeletal muscles suggests disruption of sarcomeric anchoring structures in early stage of the disease [3–5]. Even if the major role of dystrophin in maintaining the cardiomyocyte sarcolemma integrity has been revealed, there is still no clear picture on the contractile machinery network remodeling associated with dystrophin deficiency.

Although clinical interest is often related to skeletal muscle wasting and respiratory failure, DMD is often associated with

Acknowledgments: We thank Volker Baecker from the “Montpellier Ressources Imagerie” (MRI) platform and Dr. Gerard Subsol from LIRMM-CNRS Montpellier for the scientific discussions.

Conflict of interest: The authors declare no conflict of interest.

Funding: This work was supported by grants of the French Muscular Dystrophy Association (AFM; project 16073, MNM2 2012 and 20225) and the “Institut National pour la Santé et la Recherche Médicale” (INSERM) and the GDR ImaBio 2588.

*Correspondence to: O. Cazorla, PhyMedExp, Inserm U1046, CNRS UMR9214, University of Montpellier, CHU Arnaud de Villeneuve, Bâtiment Crastes de Paulet, 34295 Montpellier, Cedex 5, France.

**Correspondence to: T. Cloitre, Laboratoire Charles Coulomb, CNRS–University of Montpellier, Place Eugène Bataillon, CC074, 34095 Montpellier, Cedex 5, France.

E-mail addresses: bela.varga@umontpellier.fr, (B. Varga), albano.meli@inserm.fr, (A.C. Meli), sradoslavova.92@gmail.com, (S. Radoslavova), mathieu.panel@inserm.fr, (M. Panel), alain.lacampagne@inserm.fr, (A. Lacampagne), csilla.gergely@umontpellier.fr, (C. Gergely), olivier.cazorla@inserm.fr, (O. Cazorla), thierry.cloitre@umontpellier.fr. (T. Cloitre).

[1] These authors contributed equally to this work.

[2] Both senior co-authors.

progressive development of dilated cardiomyopathy (DCM). While established in skeletal muscle, tissue architecture remodeling in cardiac muscle remains unclear along with the occurrence of DMD-associated DCM. Using DMD dog model, namely golden retriever muscular dystrophy (GRMD), we have also shown that dystrophin deficiency leads to reduced contractility of the cardiac left ventricle [6]. Using synchrotron X-ray diffraction, we evaluated the myofilament lattice spacing and observed that dystrophin deficiency-induced chronic stress causes regional structural changes leading to heart failure [7]. We have also provided evidence in a DMD mouse model (*mdx*) that while overall cardiac dysfunction leading to heart failure appears in mice of 12-month-old, the development of DCM with aging is associated with earlier abnormal contractile properties of the ventricular cardiomyocytes [8].

It should be noted that the majority of the studies investigating DMD repercussion on cardiac muscle remodeling have employed fluorescence microscopy requiring tissue fixation and labeling with antibodies that can skew the results and interpretations. Label-free methods that maintain tissue and cell integrity and viability in a non-destructive manner are of high interest for accurate quantitative evaluation of pathological remodeling occurring in DMD.

Multiphoton microscopy has shown a great potential for *in-vitro and in-vivo* label-free imaging [9] of cells and tissues. It has many assets compared to conventional single-photon confocal microscopy for biological applications. The multiphoton excitation is only potent at the focusing volume of the objective (of the order of 0.1 μm^3), where the intensity is sufficient to generate a nonlinear response. The excitation spatial localization provides a significant photobleaching decrease. In addition, second harmonic generation (SHG) provides useful structural and optical detail of a specimen. SHG emission is at exactly half the wavelength of the light entering the material. SHG requires particular molecular orientation that is available in some highly polarizable and ordered biological systems such as large noncentrosymmetric structures. Hence, SHG microscopy has gained great interest to perform label- and fixation-free imaging of biological structures at the submicron scale [10] such as collagen, microtubules, and muscle myosin [11–13].

SHG-based images of myocytes have revealed that the source of SHG signal in the sarcomeres is not the actin or the myosin heads, but potentially the myosin tails that assemble into a hollow shaped rod structure forming the central core of thick myosin filaments [14]. Some more recent SHG-based studies contributed to the understanding of myofibrillogenesis [15], provided information on subcellular contractions [16], or contributed to evaluate the dystrophic skeletal muscle regeneration with a quantitative morphometry approach [4]. Using 3D SHG microscopy, Friedrich et al have shown that 12-month-old *mdx* skeletal fibers exhibit deranged micromorphology compromising coordinated and aligned contraction [5]. The internal disorganization in the *mdx* skeletal myofibers revealed by SHG has been correlated with altered force generation [17]. However, morphological internal changes have never been explored in DMD cardiomyocytes by SHG microscopy.

In the present study, we employed SHG microscopy to assess the impact of dystrophin deficiency and physiological calcium (Ca^{2+}) concentration on the conformational changes of the myosin filaments and cell characteristics in alive label-free *mdx* cardiomyocytes at early (4-month-old) and later (12-month-old) stage. Studies reported that at 4 months of age, the cardiac function is normal and that dysfunction of the heart appears later at 12 months old [8]. We developed a computational image analysis process allowing identification of single myofibrils. We extracted fibril-level data on the internal structure of intact cardiomyocytes acquiring details on the organization, orientation and sinuosity of its constituent individual myofibrils in presence or absence of external physiological Ca^{2+}.

We observed a structural aging-dependent remodeling in *mdx* cardiomyocytes affecting sarcomere alignment, orientation and length that could not be anticipated from standard optical imaging.

Methods

Animals and myocyte preparation

C57BL/10-Dmd^{mdx} mice were obtained from a colony maintained at a local animal facility network (RAM, Montpellier) [18]. C57BL/6 mice were obtained from Janvier Laboratories (Le Genest-Saint-Isle, France). The animals were hosted conventionally in controlled humidity and temperature, operating on 12 h of light and dark cycle with *ad libitum* food and water. All investigations conformed to the European Parliament Directive 2010/63/EU and were validated by the local ethics committee (Comité d'éthique pour l'expérimentation animale Languedoc-Roussillon, no. CEEA-LR-12078). Cardiac ventricular myocytes were enzymatically dissociated using routine procedures [19] (Figure 1, *A*). In short, we performed cervical dislocation to euthanize the mouse. The heart was then rapidly excised and retrogradely perfused at 37 °C for 6-8 min with a modified Tyrode solution [113 m NaCl, 4.7 mM KCL, 0.6 mM KH2PO4, 0.6 mM Na2HPO4, 1.2 mM MgSO4,12 mM NaHCO3, 10 mM KHCO3, 10 mM Hepes, 30 mM taurine (pH 7.4)] containing 0.1 $mg{\cdot}mL^{-1}$ of liberase (Roche) [8]. Isolated myocytes were then transferred to the same enzyme-free solution. Cardiomyocytes were maintained in the Ca^{2+}-free solution or in solution containing 1.8 mM $CaCl_2$. To avoid cell movement during acquisition, we added before acquisition to the Tyrode solution 15 mM 2,3-butanedione monoxime (BDM, ATPase inhibitor) and 10 μM blebbistatin (myosin II inhibitor) [20]. SHG acquisitions were performed within 2 h to avoid structural changes due to cell degradation after dissociation.

Second harmonic generation imaging

SHG images (Figure 1, *B*) were recorded using a custom-made multiphoton microscope setup based on a Tsunami tunable Ti:Sapphire laser (Spectra-Physics, Santa Clara, US) and an upright SliceScope microscope (MPSS-1000P) furnished with a multiphoton galvanometer scan head (MP-2000) both from Scientifica, Uckfield, UK. The Ti-Sa laser was operated in pulsed mode configuration for sample excitation, in a 760-900 nm wavelength range, at 80 MHz frequency and ~100 fs pulse duration. A Nikon CFI75 LWD-16x-W objective (NA 0.8, water immersion) was used to focus the laser beam on the sample. The SHG signal was recorded by a 1.4-NA oil-immersion condenser (U-AAC, Olympus), through a 482 nm long pass dichroic mirror (86-331, Edmund Optics) and a 447 nm high-performance band-

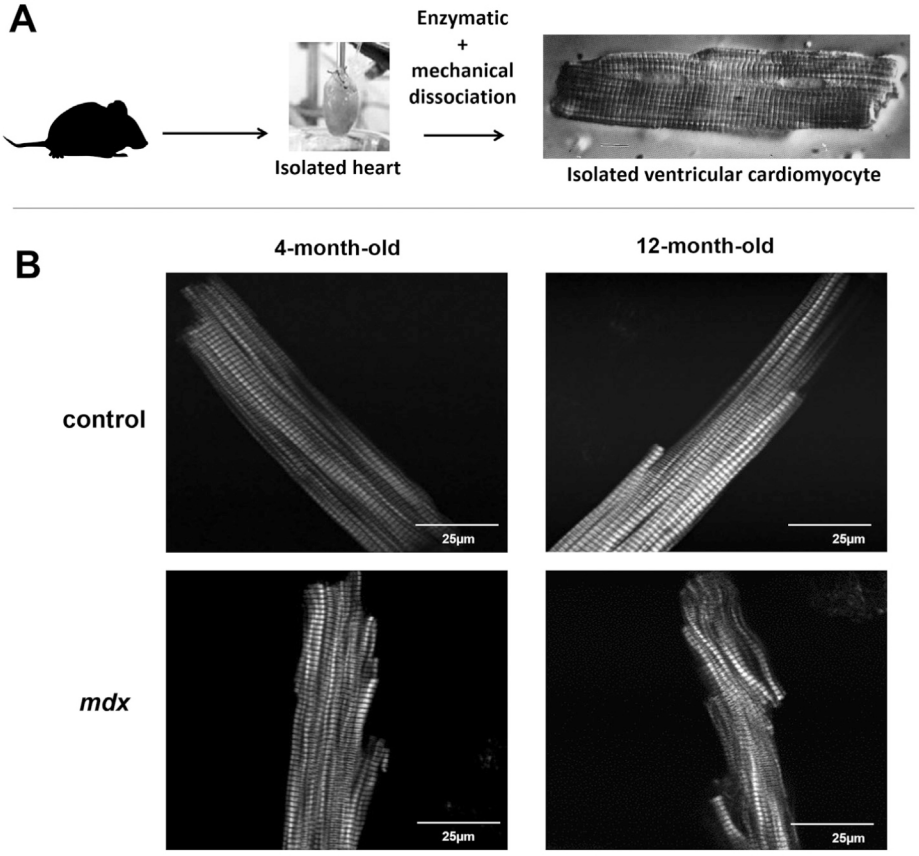

Figure 1. Second harmonic generation (SHG) imaging of intact cardiomyocytes isolated from control and *mdx* mice. **(A)**. Ventricular cardiomyocytes were isolated from the heart of control and *mdx* mice by enzymatic and mechanical dissociation. **(B)** Representative SHG images on control (top panel) and *mdx* (bottom panel) cardiomyocytes at different ages. Mature *mdx* cardiomyocytes exhibit enhanced disorder in the internal myofibrillar structure.

pass filter (48-074, Edmund Optics) and then detected by a H7422P photomultiplier (Hamamatsu). Intensity images were reconstructed from the SHG signal recorded in transmission. Image acquisitions were done in 1024 × 1024 pixel resolution at 200 line/s scanning rate.

Differential interference contrast microscopy

DIC images were recorded using a Nikon Eclipse TE2000-E inverted microscope equipped with a differential interference contrast system, using a CFI Plan 100× oil immersion objective having a 1.3 NA and 0.2 mm working distance.

Image analysis

The recorded images were subject of a semi-automated image analysis process, as presented in Figure 2. During pre-processing, first a Gaussian blur filter was applied for noise reduction, followed by a step to find and assign all local maxima in the filtered image corresponding to the M-line of the sarcomeres. The detected coordinates of local maxima were then the input of a custom-made automated algorithm aiming to build up a highly connected network by linking every point with each other. This network was afterwards progressively degraded first using maximum distance and then orientation constraints. Distance constraint threshold was defined as 2-fold the average sarcomere length (~2 µm), while the orientation constraint was settled to stay below ±30° compared to the mean orientation of the cell. After resolving the remained over connected nodes (having more than two links) and end point fusions (connected fibrils at their end), the network was clustered into single chains of points corresponding to single fibrils.

The isolated data for every individual fibril allowed the extraction of several fibril-level parameters such as sinuosity, orientation deviation, double-band percentage, double-band rate, or sarcomere length. Sinuosity was defined as the normalized length difference between the total distance (sum of sections between every consecutive point) and the beeline (distance between the start and end points) (Figure 3). Orientation of a fibril was obtained by applying a line fitting and its difference in angle from the mean orientation was defined as its deviation (Figure 3). Every link smaller than 1.4 um was defined as a double-band. Under double-band percentage we defined the ratio of double-bands in one cell, and the double-band rate is the ratio of fibrils in one cell that contains at least one double-band. The sarcomere length of a fibril was defined as the mean distance between consecutive points, omitting double-bands, while cell width measurements were done manually in ImageJ.

Data analysis, statistics and interpretation

Basic image treatment and the pre-processing were done in Fiji (an ImageJ distribution) [21], while the custom-made script

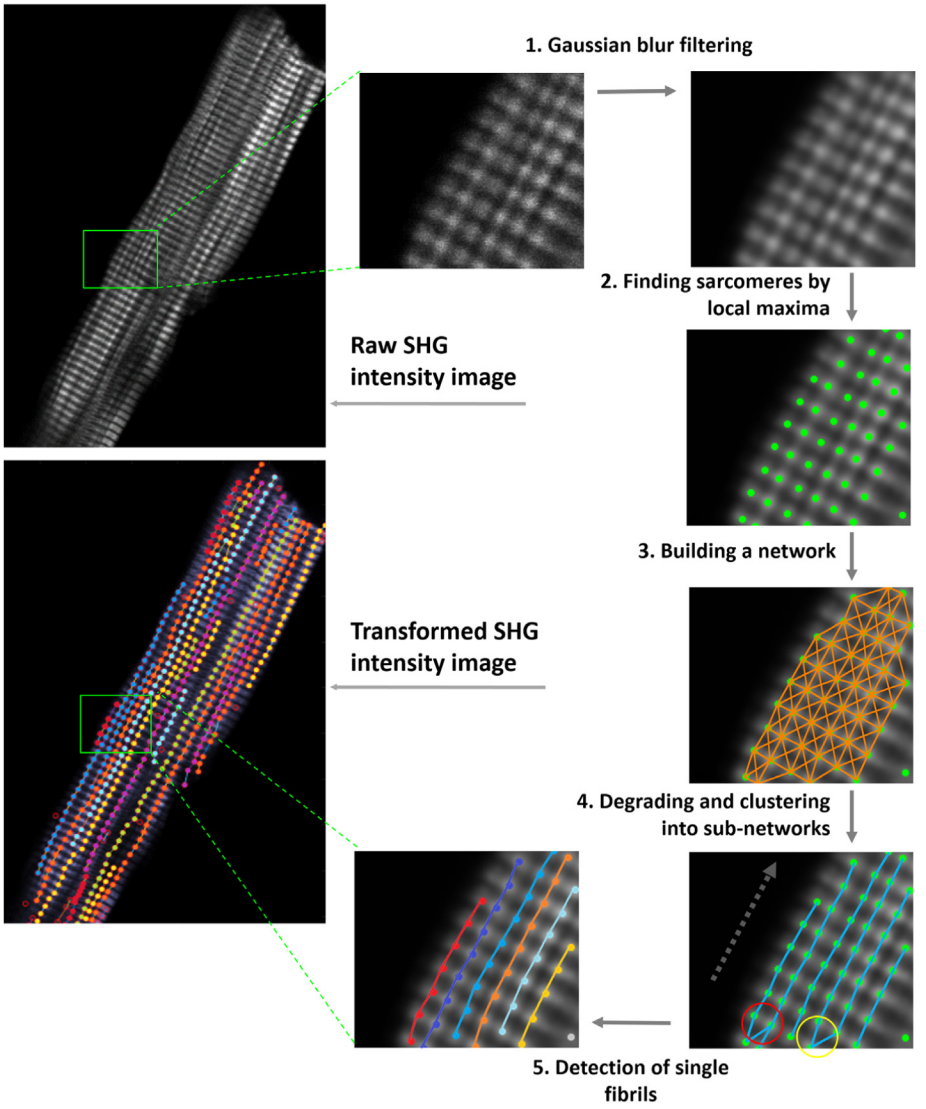

Figure 2. Data processing work flow. After applying a Gaussian filter on the recorded SHG intensity images (step 1), the sarcomeres were detected by finding local maxima (step 2). These were considered as nodes of a network. The obtained highly connected network (step 3) of all sarcomeres was degraded using distance and orientation constraints (step 4) and clustered into single fibrils (step 5). This allowed the extraction of fibril-level parameters, such as orientation dispersion, sinuosity, sarcomere length and double-band related parameters.

for the automated fibril-level data extraction was written in Matlab (MathWorks, Natick, USA).

Statistical analysis was carried out using SigmaPlot (Systat Software, San Jose, USA). The significance was determined by unpaired Student *t* test and two-way ANOVA followed by a Holm-Sidak *post hoc* test, respectively. All data are reported as box plots, with interquartile range from 25% to 75%, where the middle line represents the median, while the red square is the mean of the data. We considered a statistical difference when $P < 0.05$.

Results

The SHG signal of control and mdx cardiomyocytes reveals internal structural alterations with aging

Intact cardiomyocytes were isolated from the hearts of 4- and 12-month-old control and mdx mice by enzymatic digestion (Figure 1, *A*). In order to obtain high quality SHG images in alive cardiomyocytes avoiding artifacts induced by spontaneous contractions, the experiments were carried out in presence of the ATP-ase inhibitor butanedione monoxime (BDM) and the myosin inhibitor blebbistatin [20]. During exploratory SHG acquisitions, control and *mdx* cardiomyocytes of young animals (4-month-old) had visually roughly similar internal structure (Figure 1, *B*, left panels). Interestingly, in older animals (12-month-old), SHG signal of mdx cardiomyocytes was noticeably different to control myocytes with curvier myofibrils (Figure 1, *B*, right panels). This would suggest potential remodeling of the internal structure with aging in mdx cardiomyocytes. To quantify those changes, we developed a custom-made automated image analysis algorithm. The process is illustrated in Figure 2 and detailed in Materials and Methods. Briefly, after noise reduction on the recorded SHG intensity images, the sarcomeres were detected by finding local maxima. These points were then considered as nodes of a network.

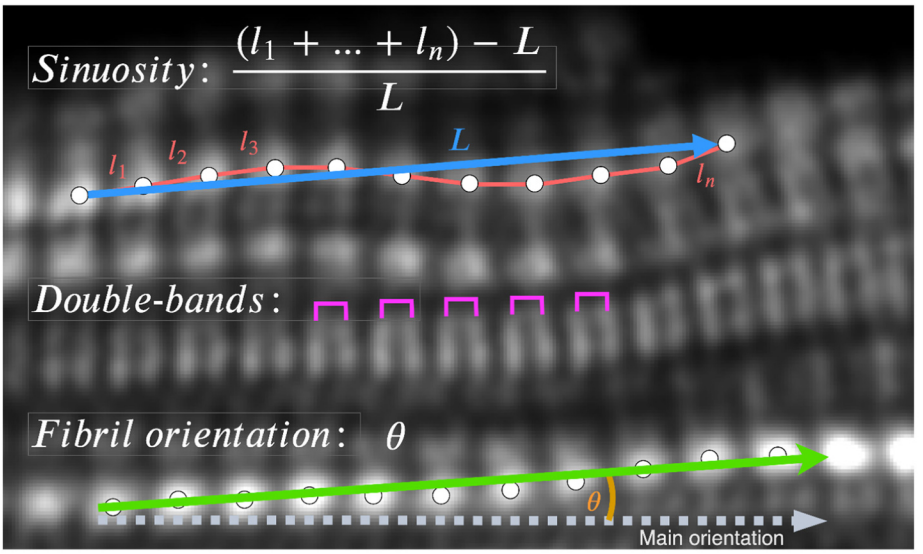

Figure 3. Sinuosity, double-band and fibril orientation. Sinuosity, defined as the difference between the real length of the fibril and the beeline between the two ends of the fibril, normalized with the beeline. **Double-bands**, defined as smaller then 2/3rd of a usual sarcomere length. **Fibril orientation**, defined as the angle between the fitted line on the detected sarcomeres and the mean orientation of all fibrils.

The obtained highly connected network of all sarcomeres was degraded using distance and orientation constraints and clustered into single fibrils. With the algorithm, we could extract different fibril-level structural parameters of the contractile machinery such as fibril orientation, sinuosity, sarcomere length, and, so called, double-bands that characterize the heavy myosin chain organization (for detailed description see Materials and Methods and Figure 3). By fibril orientation we aimed at evaluating the ordering level inside single cardiomyocytes, while sinuosity served to quantify the curviness of the fibrils. From the myosin chain organization, we aimed at quantifying the presence of double-bands in the myocytes. This characteristic was previously associated with multiple factors and considered as an intrinsic characteristic, through relating it to external factors, up to linking them to internal structure disorganization [5,22–24].

SHG signal is not affected by the extracellular Ca^{2+} concentration

Intracellular calcium concentration depends on the extracellular calcium concentration. The effect of intracellular calcium content on SHG signal in cardiomyocytes or myocyte in general has never been tested. During the process of cell isolation, the external [Ca^{2+}] is progressively raised from 0 mM to 1.8 mM Ca^{2+} that should increase the internal calcium concentration. When released in the cytosol, calcium interacts with troponin C on the actin thin filament. This interaction induces a change of the conformation of the thin filaments to let the myosin head to bind. This change of conformation of the thin filaments still exists in presence of BDM and blebbistatin because both act on the myosin ATPase. Whether this change of thin filament conformation alters SHG signal is unknown. We first tested whether the presence of extracellular Ca^{2+} at physiological concentration modulates the structure and sarcomere organization visible through SHG microscopy. We hypothesized that the presence of Ca^{2+} inside the myocyte may affect the conformation of the thin filaments, number of actin-myosin cross-bridges formed and thus the SHG signal. Freshly dissociated ventricular cardiomyocytes were imaged by SHG microscopy both in normal solution containing 1.8 mM Ca^{2+} and in external Ca^{2+}-free solution, which consequently decreases the internal Ca^{2+} concentration. This test has been performed with old adult control mice. We found that the decrease in extracellular Ca^{2+} did not change the sarcomere length nor the orientation of the sarcomeres of control myocytes (Figure 4, *A* and *B*). Myocytes were perfectly relaxed as indicated by the slack sarcomere length of 1.97 ± 0.04 and 1.96 ± 0.04 µm measured in 1.8 mM Ca^{2+} and Ca^{2+}-free respectively (Figure 4, *A* and *B*), values consistent with known values published in the literature (see all exact data in Table 1). The sinuosity of the acquired heavy myosin chain signal was unchanged in presence of Ca^{2+} with no significant difference in double-band percentage and rate (Figure 4, *C-E*). Similar results on the effect of external [Ca^{2+}] were obtained with old *mdx* myocytes (Figure 4, *F-J*). Accordingly, all the following presented results were obtained in physiological conditions in a solution containing 1.8 mM Ca^{2+}.

Aging causes increased sarcomere length and decreased cell width in dystrophin-deficient cardiomyocytes

Using 3D SHG microscopy, Friedrich et al have revealed that dystrophin-deficiency leads to disturbed micromorphology compromising coordinated and aligned contraction in 12-month-old *mdx* skeletal fibers [5]. We next assessed whether aging could similarly affect the structure and sarcomere organization of the *mdx* cardiomyocytes. To that, we compared freshly dissociated intact control and *mdx* cardiomyocytes of 4- and 12-month-old. Aging caused a sarcomere length decrease from 1.99 to 1.96 µm and a cell width increase from 22.6 to 26.7 µm in control cardiomyocytes (Figure 5). Such changes were not observed in dystrophin-deficient cardiomyocytes. Mean

Table 1
Mean ± standard deviation of all measured parameters.

	Orientation dispersion (°)	Sinuosity (%)	Double-band percentage (%)	Double-band rate (%)	Sarcomere length (μm)	Cell width (μm)
1.8 mM $[Ca^{2+}]_{ext}$						
Control 4 mo	**3.1 ± 1.1** [a]	**0.69 ± 0.26**	21.6 ± 19.2	43.4 ± 23.7	**1.99 ± 0.04** [d]	**22.3 ± 5.6** [f]
Control 12 mo	**2.5 ± 0.8** [a,b]	**0.63 ± 0.2** [c]	15.9 ± 11.3	38.1 ± 20.0	**1.96 ± 0.04** [d,e]	**25.0 ± 4.5** [f,g]
mdx 4 mo	**3.0 ± 1.1**	**0.75 ± 0.26**	15.7 ± 11.3	39.0 ± 18.5	**2.00 ± 0.05**	**21.1 ± 6.4**
mdx 12 mo	**3.5 ± 1.4** [b]	**0.76 ± 0.21** [c]	15.9 ± 8.9	40.5 ± 14.5	**1.99 ± 0.06** [e]	**20.3 ± 3.6** [g]
0 mM $[Ca^{2+}]_{ext}$						
Control 4 mo	3.1 ± 0.9	0.82 ± 0.23	12.7 ± 13.6	34.4 ± 25.5	2.02 ± 0.06	20.9 ± 4.1
Control 12 mo	2.7 ± 0.7	0.68 ± 0.14	19.9 ± 11.2	44.4 ± 17.9	1.97 ± 0.04	21.3 ± 5.7
mdx 4 mo	2.9 ± 1.0	0.69 ± 0.14	16.8 ± 11.5	40.6 ± 18.5	2.00 ± 0.07	21.4 ± 5.4
mdx 12 mo	3.4 ± 1.2	0.74 ± 0.19	19.1 ± 6.9	47.5 ± 15.7	2.00 ± 0.04	22.8 ± 8.1

Bold values correspond to the parameters where significant changes have been observed. Where indicated, identical exponent letters show significant differences between the marked values.

sarcomere lengths for both *mdx* and control cardiomyocytes from young animals were similar, very close to 2 μm, as well as cell width value distributions with mean values around 22 μm. In old animals, sarcomere length was higher in *mdx* cardiomyocytes when compared to age-matched control cells (Figure 5, *B*). Interestingly, cell width was unchanged with aging in *mdx* cells and was smaller compared to age-matched control cardiomyocytes (Figure 5, *C*).

Aged mdx cardiomyocytes exhibit further structural and sarcomere alterations

When exploring the sarcomere organization, sinuosity of the myofibrils of control and *mdx* cardiomyocytes did not differ with aging (Figure 6, *B*). No statistical difference was observed in the sinuosity between young *mdx* and control population. The orientation dispersion was also identical for both control and *mdx* 4-month-old cardiomyocytes with an average value of about 3.1° (Figure 6, *C*). In addition, the orientation dispersion decreased with aging only in control cells but not in *mdx* cells. In old animals, *mdx* cardiomyocytes displayed higher percentage of sinuosity and orientation dispersion compared to age-matched control cardiomyocytes (Figure 6, *B* and *C*). Aging did not alter the double-band percentage and rate in any group (Figure 6, *D* and *E*). The mean and standard deviation values of the extracted parameters (Figures 5 and 6) are gathered in Table 1. We observed no significant difference in any of the extracted parameters when comparing data between *mdx* and control cardiomyocytes, coming from young animals.

Altogether, the SHG data indicate that the cardiomyocytes of old *mdx* mice exhibited longer sarcomere lengths and are thinner by about 30% compared with control myocytes. In addition, their mean fibril sinuosity and orientation dispersion were significantly increased compared to the control cells by about 19% and 44%, respectively, indicative of internal disorganization of the myofibrils.

In order to stress the appropriateness of SHG microscopy for such study and to demonstrate that the alive cardiomyocyte internal structure changes in old *mdx* mice can only be revealed by SHG analysis, we acquired images of the cardiomyocytes from young and old mice with differential interference contrast (DIC) microscopy (Figure 7). DIC imaging provides a good contrast for the eye. However, as the origin of the contrast is linked to the difference in the optical paths, it does not provide true intensity signal and could not serve for image processing, especially for fibril level data extraction. More importantly, we were unable to detect any structural changes from the images between young and old animals (Figure 7, *B*). They looked perfectly normal, which contrasts with the images obtained using SHG analysis (Figure 7, *A*). Altogether, our results indicated the great potential of SHG in evaluating the age-dependent deterioration of myofibrils within alive and intact *mdx* cardiomyocytes.

Discussion

Our work demonstrates the great potential of nonlinear optics to reveal biological/structural modifications induced by a severe illness. DMD is one of the worst debilitating neuromuscular disorders causing death prior 30 years old due to respiratory and/or cardiac failure. While the skeletal muscle dystrophinopathies have been explored, the consequences of dystrophin deficiency on the cardiac muscle degeneration in link with the lethal development of DCM are unclear. In the present study we revealed, for the first time in cardiac myocytes, the interest in using SHG to evaluate the progressive intracellular and sarcomeric remodeling induced by dystrophin-deficiency with age. Our experimental conditions allowed acquisition of images of the internal structure of intact alive cardiomyocytes, avoiding artifacts associated with cell fixation and antibody binding. Using a custom-made image analysis, we evaluated the cell structure at the single myofibril level.

Considering the key role of Ca^{2+} in the cardiac muscle contraction *via* sarcomere shortening, we first tested the impact of physiological Ca^{2+} concentration on the myosin SHG signal in control cardiomyocytes. We obtained no conclusive effect of extracellular Ca^{2+} concentration on the internal structure, orientation, sinuosity or myosin arrangement. These results suggested that, although we employed experimental conditions to maintain the cardiomyocytes alive, the biophysical properties

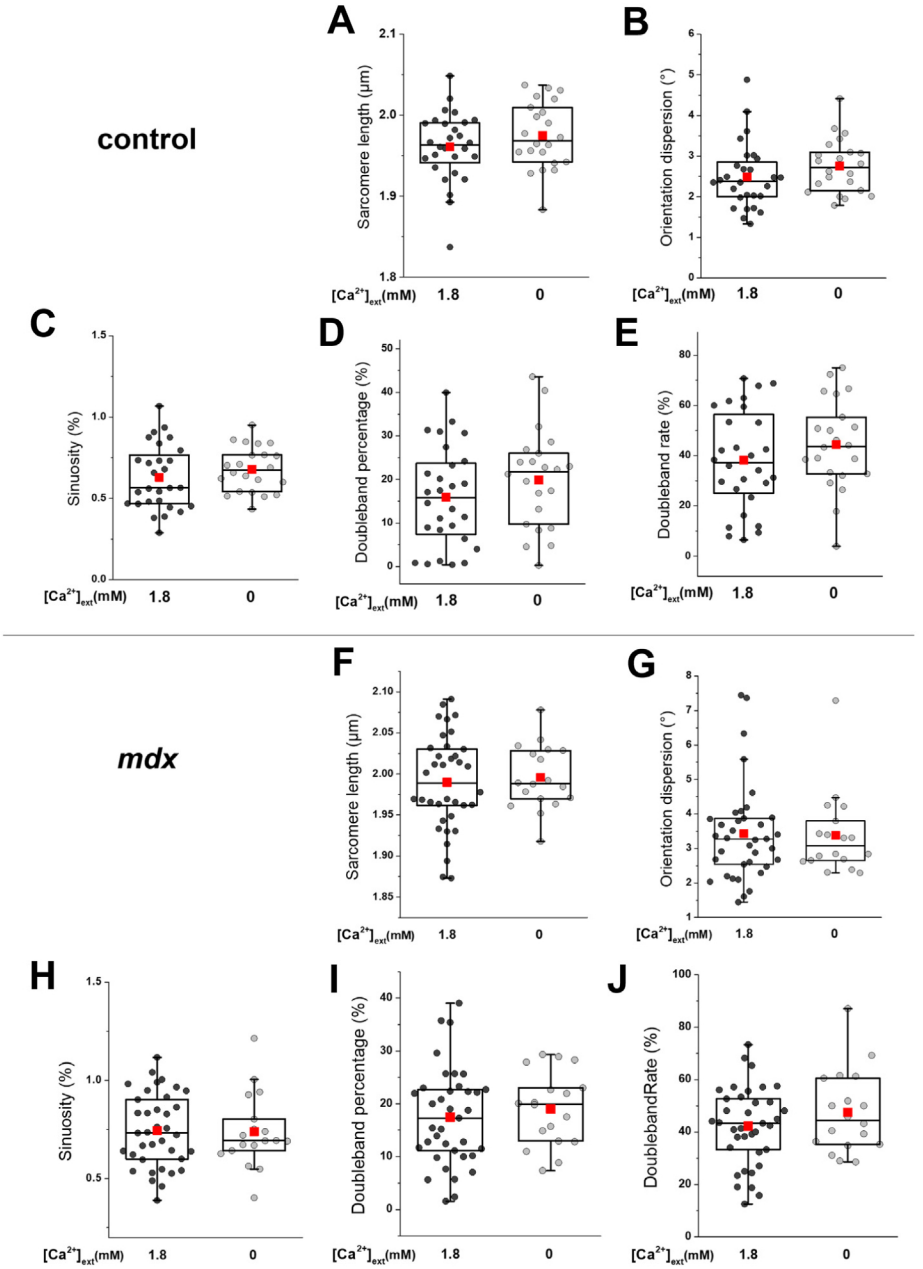

Figure 4. Effect of external Ca^{2+} concentration on the extracted parameters from SHG images measured on 12-month-old control/*mdx* cardiomyocytes. SHG images were obtained from cardiomyocytes maintained in 1.8 mM Ca^{2+} (black dots) or Ca^{2+} free (gray dots) external physiological solution. No significant effect of external Ca^{2+} was observed on the extracted parameters (n = 28 myocytes (3 animals) for control with Ca^{2+} and n = 22 myocytes (3 animals) for control without Ca^{2+}; n = 37 myocytes (5 animals) for *mdx* with Ca^{2+} and n = 18 myocytes (3 animals) for *mdx* without Ca^{2+}).

of the sarcomere resulting from SHG signal are not modulated by the presence of Ca^{2+}. We purposely performed these experiments on alive cardiomyocytes, inhibiting spontaneous contraction by BDM and blebbistatin to facilitate acquisition of high quality SHG images. Indeed, by inhibiting acto-myosin interaction, it fully relaxes the myocyte, independently of the amount of diastolic calcium level. Our present experimental conditions are ideal and required to precisely examine sarcomere structure in particular the diastolic sarcomere length and width as we showed previously [25]. Furthermore, Plotnikov et al have demonstrated that only myosin rod domains are responsible for the SHG signal in skeletal muscle fibers [14]. They also observed that SHG spectroscopy cannot sense muscle contraction as it does not induce any difference in the intensity or polarization of the signal. These features may be similar in cardiac muscle, explaining the unchanged SHG signal recorded on cardiomyocytes obtained in presence or absence of physiological extracellular of Ca^{2+}. Here, the increase in intracellular Ca^{2+} concentration was expected to further activate the thin-filaments (actin filaments). Indeed, Ca^{2+} binds to troponin C, which causes conformational changes of the thin filaments. Our results confirmed that the SHG signal is not altered by any change of

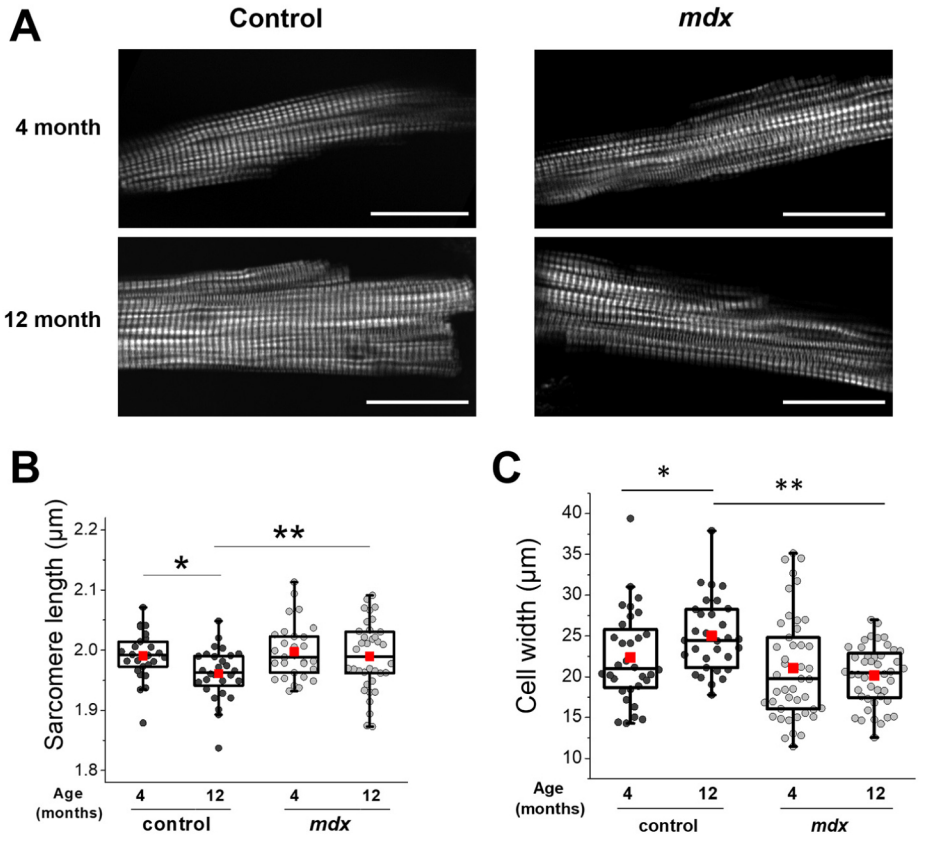

Figure 5. Structural cellular analysis of SHG images from young and old control and *mdx* cardiomyocytes. **(A)** Representative SHG images of the corresponding conditions. **(B)** Significant differences in **sarcomere length** were observed between young and mature control cells, as well as between mature control and mature *mdx* cardiomyocytes (n = 26 myocytes (3 animals) for control at 4 months and n = 28 myocytes (3 animals) for control at 12 months; n = 29 myocytes (5 animals) for *mdx* at 4 months and n = 37 myocytes (5 animals) for *mdx* at 12 months). **(C)** Significant differences have been observed in **cell widths** of young and mature control cells, as well as mature control and mature *mdx* cardiomyocytes. In addition, overall significant differences were found between control and *mdx* for both parameters (n = 32 myocytes (3 animals) for control at 4 months and n = 31 myocytes (3 animals) for control at 12 months; n = 45 myocytes (5 animals) for *mdx* at 4 months and n = 43 myocytes (5 animals) for *mdx* at 12 months). *, $P < 0.05$; **, $P < 0.01$, two-way ANOVA.

the thin filaments. These experiments in different external Ca^{2+} concentrations confirmed also that the internal structure was not altered by the progressive increase to 1.8 mM Ca^{2+} during the process of cell isolation. This was true for both control and *mdx* cardiomyocytes. Indeed, it was previously shown that basal level of calcium concentration is increased in old *mdx* mice [8]. Meantime, like in many cardiomyopathies associated with higher intracellular Ca^{2+} concentration, the content and/or activity of intracellular calcium-dependent proteases such as calpains are increased. This has been shown in a utrophin/dystrophin deficiency mouse model, a more severe myopathy model than *mdx* [26]. The absence of SHG signal change in presence or absence of physiological Ca^{2+} concentration indicated no Ca^{2+}-dependent activation of the proteases leading to structural defaults and ruled out any artifact of the myosin signal change associated to protease activation in both control and *mdx* cardiomyocytes.

Control cardiomyocytes displayed changes between 4- and 12-month-old with regard to sarcomere length, cell width and fibril orientation dispersion. This reflects a physiological adaptation of the cardiomyocytes certainly due to increased workload of the heart [27]. We observed that the cellular internal structure likely becomes more organized at 12 months old, showing slightly decreased sinuosity and more aligned myofibril structure compared to younger counterparts. Importantly, the shorter sarcomere length and enlarged cell width as well as the decreased orientation dispersion suggest a maturating process towards adult cardiomyocytes. These results on potential maturation of the sarcomeres are supported by previous studies, in which sarcomere lengths of skeletal muscle fibers were used to monitor myofibrils assembly in alive cells [14,28]. The basal sarcomere length shortening observed here with aging in control myocytes could be explained by expression variations in the different isoforms of the sarcomeric elastic protein, titin, during sarcomere development. Titin length is a major contributor of the sarcomere length and of the intracellular stiffness [29]. With aging, the adult normal heart expresses a short titin isoform leading to a decreased sarcomere length and a higher cardiac stiffness [30].

According to our findings, all structural parameters both for control and *mdx* are similar in young animals. Their structural disorganization level, quantified by sinuosity and orientation dispersion, as well as their dimension related characteristics, such as cell width and sarcomere length, is similar. In other words, at early stage, based on the SHG measured parameters, the *mdx* cardiomyocytes are structurally not distinguishable from

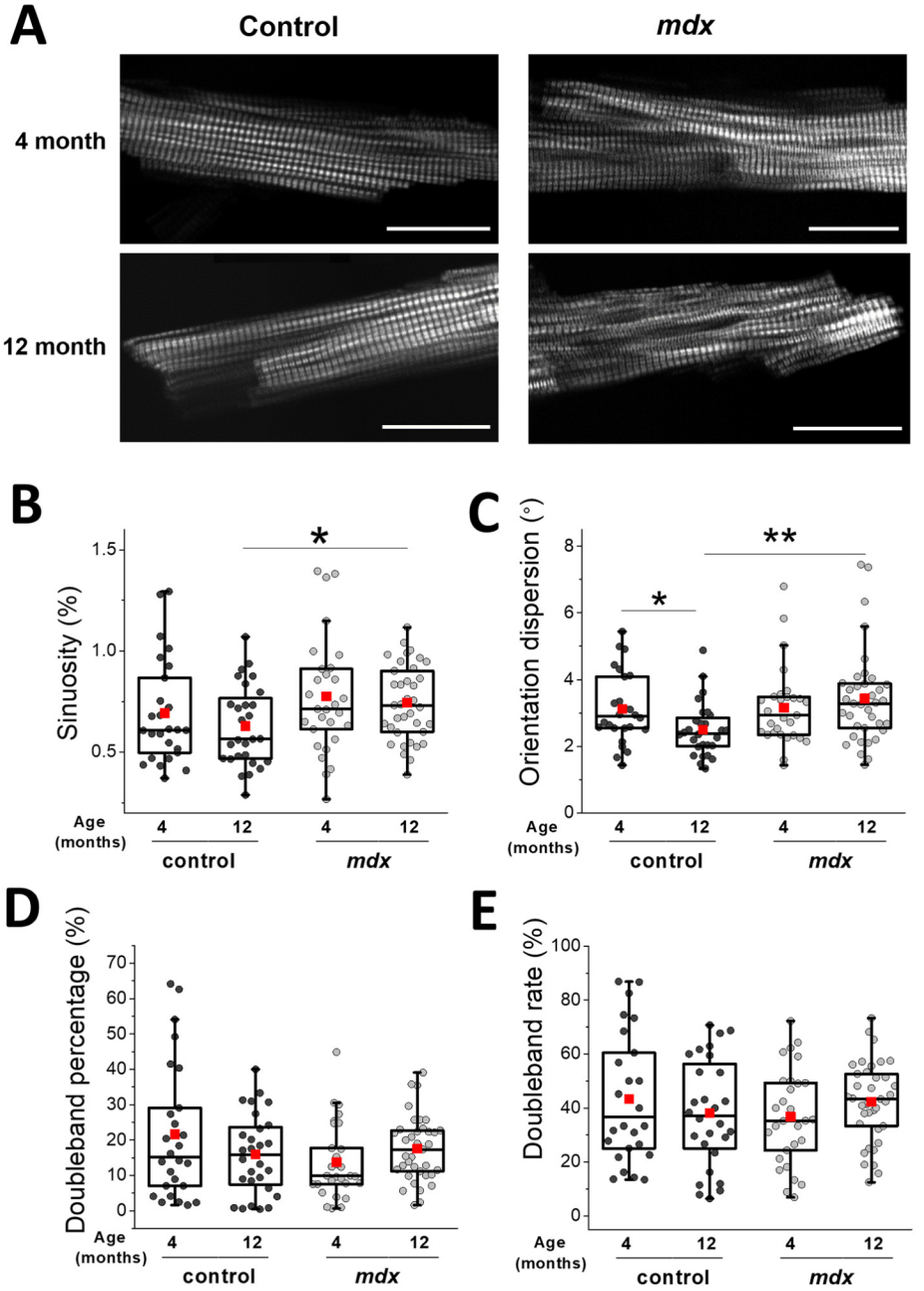

Figure 6. Myofibrillar rearrangement in control and *mdx* cardiomyocytes with aging. **(A)** Representative SHG images of the corresponding conditions. Average sinuosity **(B)** and orientation dispersion **(C)** of myofibrils within each cardiomyocyte, present significant differences between mature control and mature *mdx* cells. Average double-band percentage **(D)** and rate **(E)** of the myofibrils within each cardiomyocyte are not significant. In case of sinuosity and orientation dispersion overall significant differences have been also observed between control and *mdx* cardiomyocytes. (n = 26 myocytes (3 animals) for control at 4 months and n = 28 myocytes (3 animals) for control at 12 months; n = 29 myocytes (5 animals) for *mdx* at 4 months and n = 37 myocytes (5 animals) for *mdx* at 12 months). *, $P < 0.05$; **, $P < 0.01$; two-way ANOVA.

control ones. This does not mean that the *mdx* cardiomyocytes are healthy at this age. Indeed, we have shown defects in the intracellular Ca^{2+} cycling in particular an increase in the level of Ca^{2+} concentration at rest in 1-month-old *mdx* mouse cardiomyocytes [8]. These early defaults in Ca^{2+} homeostasis may trigger intracellular remodeling. Indeed, at the age of 6 months, we observed a decrease in the neuronal nitric oxide synthase (NOS) expression and increase in inducible NOS expression compared with control and 1-month-old *mdx* cardiomyocytes. The elevation of inducible NOS expression is classically associated with cardiomyopathies.

Our study revealed progressive structural differences between *mdx* compared with control cardiomyocyte at a mature stage (12-month-old) with thinner *mdx* cardiomyocytes displaying longer sarcomeres associated with more tortuous and diversely oriented fibrils. These new findings support the concept that dystrophin-deficiency causes cardiac muscle degeneration at a later stage as a major difference with DMD skeletal muscle loss at early-stage

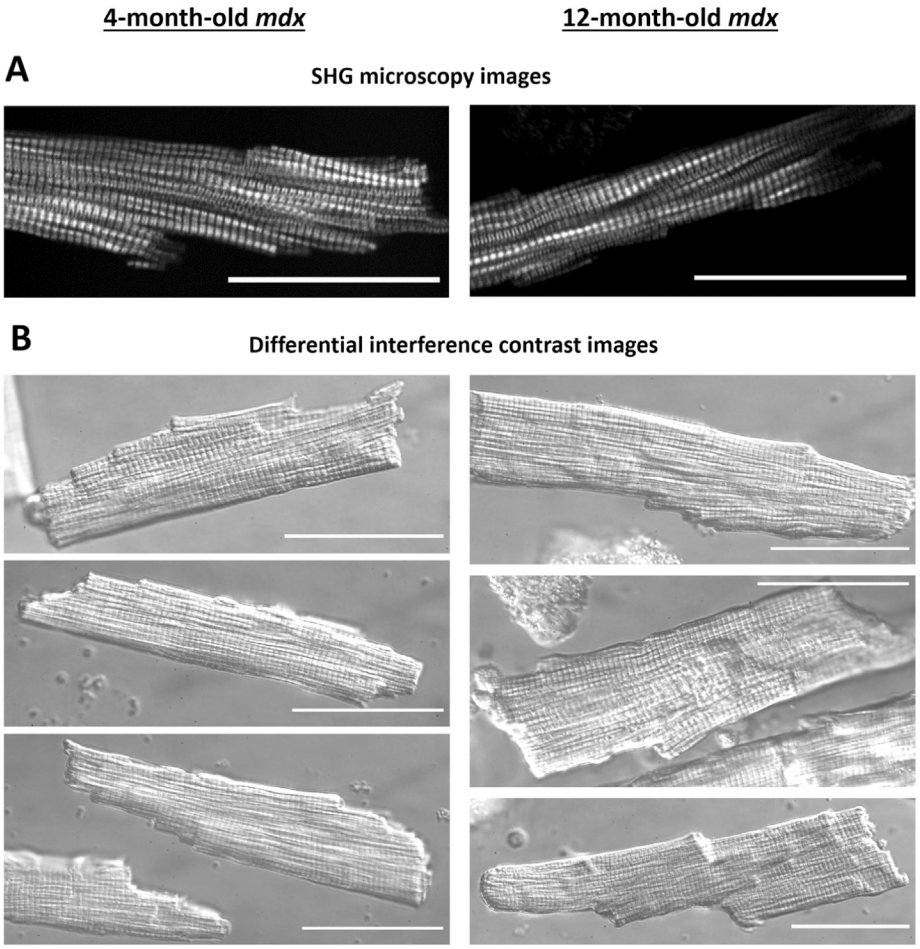

Figure 7. Comparison of SHG and Differential interference contrast (DIC) microscopy images of *mdx* cardiomyocytes. **(A)** SHG images on 4- and 12-month-old mice cardiomyocytes presenting high background to signal contrast and true myosin intensity signal, being highly appropriate for image processing. **(B)** DIC images on corresponding cardiomyocytes provide good contrast for the eye; however, as the contrast is linked to optical path difference, it could hardly serve for image processing, especially for fibril level data extraction. All scale bars are 50 µm.

[7,31]. They indicate a structural and progressive damage of the myofibrils that was not induced by the procedure of cell dissociation. They also strongly support that the structural disorganization of the myofibrils in *mdx* cardiomyocytes causes an uncoupled and dysfunctional myofibrillar network likely leading to progressive reduced contraction force and eventually hypocontractility as a major feature of the DMD-associated dilated cardiomyopathy. Similar findings, revealed by SHG in *mdx* skeletal muscle fibers, indicated that myofibril tilting and twisting cause a reduced contraction force of at least 20% [5].

The longer sarcomere length in old *mdx* cardiomyocytes could be due to the expression of a longer titin isoform that could reduce the stiffness of the myocytes [32]. This could explain why a previous study reported that old *mdx* mice have a more compliant heart than the age-matched control mice [33]. Our present results indicate that the cardiac sarcomere alignment, orientation and length are progressively affected by the absence of dystrophin with no visible consequences at early-stage (4 months old) compared to a known disease stage (12 months old) related to cardiac dysfunction and progressive DCM as we have previously showed [8].

Furthermore, our findings are also supported by our earlier study showing that the myofilament structure and function are altered in GRMD dogs [7]. Li et al [34] showed that myocyte fractional shortening is higher at 4 months of age in *mdx* compared with control mice being associated with higher calcium release during contraction. This is confirmed by other groups showing that young *mdx* animals have increased calcium current and intracellular calcium transient [36,38,40]. The higher cellular contractility in young animals is supposed to compensate cell death and maintain normal global cardiac contraction. With aging (12 months), the amplitude of cellular contraction of *mdx* cardiomyocytes decreases compared with 4 months of age and reaches similar level than control cardiomyocytes [34]. Thus, at this stage, *mdx* myocytes cannot compensate cell death that occurs at a higher rate (more fibrosis) and thus global contractility is decreased (hypocontractility). This is also in line with reports on myofilament and mitochondrial defects in DCM [35,37] and DMD patient derived cardiomyocytes [39].

The distortion of the myofibrils may be induced by a process of dedifferentiation as observed in myocardial remodeling in heart failure. In fact, morphological rearrangement of cardiomyocytes is

a protective remodeling for adaptation [41]. Loss of features of cell maturity, including de-sarcomerization and myofibril de-organization and re-expression of fetal genes, has been reported in pathophysiological contexts [42,43].

The distortion of the myofibrils may be induced by gradual changes of other intracellular organelles. Interestingly, age dependent changes in mitochondrial morphology were shown in *mdx* hearts [44]. Transmission electron micrographs revealed mitochondrial increased area and loss of normal cristae structure in adult *mdx* cardiac muscle. Meantime, it was shown that changes in mitochondria volume can mechanically affect morphological as well as functional properties of intracellular organelles, including myofilaments and nuclei [45]. Mitochondria are also dynamic structures capable of fission and fusion under stress [46]. Whether those changes in mitochondria morphology are responsible for the myofilament misalignment remains to be determined.

Finally, our study shows a default of coupling between myofibrils. In the cardiomyocytes, intermediate filaments, especially desmin, form an extended scaffold linking the entire contractile apparatus to several membranous compartments (*i.e.*, sarcolemma costameres and desmosomes of the intercalated disks) and organelles (*i.e.*, sarcoplasmic reticulum, mitochondria, nucleus and lysosomes). In dystrophin-deficient mice, desmin expression is increased and may contribute to a compensatory mechanism [47]. The lack of desmin in the heart leads to cardiomyocyte hypertrophy and reduction in active force generation [48]. Whether the intermediate filaments and desmin play a role in the myofibrillar distortion we observed requires further experiments.

We also quantified the SHG signal of double-bands in the cardiomyocytes. As reported previously for DMD fixed and stained skeletal muscle cells [5,49], the appearance of double SHG bands can be related to the internal structural characteristics of myofibers, to disorganization among the fibrils [24] and sarcomere pattern irregularities. Other species such as frog and rabbit also exhibit a double-band signal from their cardiomyocytes and were considered as an intrinsic characteristic of the sarcomeres [22,50]. Nevertheless, other studies reported that occurrence of double-bands can also be the consequence of external factors such as stretching or laser irradiation [23,24]. Although the double-band percentage and rate were considered as promising parameters to reveal structural modifications, our data obtained on alive and intact cardiomyocytes show that the double-band proportion was unaffected by the aging and DCM-induced dystrophin deficiency. Therefore, we concluded that double-band parameters are not relevant indicators to follow structural changes in cardiomyocytes with large scale SHG microscopy, most likely due to the combined ordered- and disordered-state origin of double-band signals together with the highly nonlinear SHG effect.

Altogether, our findings confirmed the great potential for SHG in evaluating the age-dependent deterioration of myofibrils within alive and intact *mdx* cardiomyocytes. For the first time, we provided structural information on the contractile machinery disorganization in alive *mdx* cardiac tissue that could not be detected by other imaging procedures. Further work with non-invasive approaches to directly monitor structural changes in alive cardiomyocytes is certainly needed to better understand DMD-associated DCM development enabling also to decipher the processes underlying the disease progression. Our work provided valuable quantitative structural parameters to monitor DMD related modifications in alive and intact cardiomyocytes. Overall, our findings may help to identify novel early-stage biomarkers of the DCM progression in DMD patients but also for all other origins of DCM.

Author contributions

ACM, TC, MP and SR performed the experiments on the mice and cardiomyocytes. BV performed the data and statistical analysis. ACM, OC and AL provided the biological and physiological expertise. BV, CG and TC provided the expertise in physics, microscopy and automated data analysis. BV, ACM, CG and OC wrote the manuscript. ACM, CG, OC and TC designed the study and interpreted the data. All authors provided critical review of the manuscript and approved its submission.

References

1. Cullen MJ, Fulthorpe JJ. Stages in fibre breakdown in Duchenne muscular dystrophy an electron-microscopic study. *J Neurol Sci* 1975;**24**:179-200.
2. Matsuda R, Nishikawa A, Tanaka H. Visualization of dystrophic muscle fibers in mdx mouse by vital staining with Evans blue: evidence of apoptosis in dystrophin-deficient muscle. *J Biochem* 1995:959-64.
3. Brouilly N, Lecroisey C, Martin E, Pierson L, Mariol M, Qadota H, et al. Ultra-structural time-course study in the C. elegans model for Duchenne muscular dystrophy highlights a crucial role for sarcomere-anchoring structures and sarcolemma integrity in the earliest steps of the muscle degeneration process. *Hum Mol Genet* 2015;**24**(22):6428-45.
4. Buttgereit A, Weber C, Friedrich O. A novel quantitative morphometry approach to assess regeneration in dystrophic skeletal muscle. *Neuromuscul Disord* 2014;**24**(7):596-603.
5. Friedrich O, Both M, Weber C, Schrümann S, Teichmann MDH, Wegner F, et al. Microarchitecture is severely compromised but motor protein function is preserved in dystrophic mdx skeletal muscle. *Biophys J* 2010;**98**(February):606-16.
6. Su JB, Cazorla O, Blot S, Blanchard-Gutton N, Sambin L, Sampedrano CC, et al. Bradykinin restores left ventricular function, sarcomeric protein phosphorylation, and e/nNOS levels in dogs with Duchenne muscular dystrophy cardiomyopathy. *Cardiovasc Res* 2012;**95**:86-96.
7. Ait Mou Y, Lacampagne A, Irving T, Scheuermann V, Blot S, Ghaleb B, et al. Altered myofilament structure and function in dogs with Duchenne muscular dystrophy cardiomyopathy. *J Mol Cell Cardiol* 2018;**114** (November 2017):345-53.
8. Fauconnier J, Thireau J, Reiken S, Cassan C, Richard S, Matecki S, et al. Leaky RyR2 trigger ventricular arrhythmias in Duchenne muscular dystrophy. *Proc Natl Acad Sci* 2010;**107**(4):1559-64.
9. Zipfel WR, Williams RM, Webb WW. Nonlinear magic: multiphoton microscopy in the biosciences. *Nat Biotechnol* 2003;**21**(11):1369-77.
10. Sivaguru M, Kabir MM, Garita MR, Biggs DSC, Sivaguru BS, Sivaguru VA, et al. Application of an advanced maximum likelihood estimation restoration method for enhanced-resolution and contrast in second-harmonic generation microscopy. *J Microsc* 2017;**267**(3):397-408.
11. Yuan C, Wang Z, Borg TK, Ye T, Baciu C, Bradshaw A, et al. Changes in the crystallographic structures of cardiac myosin filaments detected by polarization-dependent second harmonic generation microscopy. *Biomed Opt Express* 2019;**10**(7):3183-95.

12. Dubreuil M, Tissier F, Le Roy L, Pennec JP, Rivet S, Giroux-Metges MA, et al. Polarization-resolved second harmonic microscopy of skeletal muscle in sepsis. *Biomed Opt Express* 2018;**9**(12):6350-8.
13. Syverud BC, Mycek MA, Larkin LM. Quantitative, label-free evaluation of tissue-engineered skeletal muscle through multiphoton microscopy. *Tissue Eng - Part C Methods* 2017;**23**(10):616-26.
14. Plotnikov SV, Millard AC, Campagnola PJ, Mohler WA. Characterization of the myosin-based source for second-harmonic generation from muscle sarcomeres. *Biophys J* 2006;**90**(2):693-703.
15. Liu H, Shao Y, Qin W, Runyan RB, Xu M, Ma Z, et al. Myosin filament assembly onto myofibrils in live neonatal cardiomyocytes observed by TPEF-SHG microscopy. *Cardiovasc Res* 2013;**97**:262-70.
16. Awasthi S, Izu LT, Mao Z, Jian Z, Landas T, Lerner A, et al. Multimodal SHG-2PF imaging of microdomain Ca-contraction coupling in live cardiac myocytes. *Circ Res* 2015;**118**(2):19-28.
17. Schneidereit D, Nübler S, Prölß G, Reischl B, Schürmann S, Müller OJ, et al. Optical prediction of single muscle fiber force production using a combined biomechatronics and second harmonic generation imaging approach. *Light Sci Appl* 2018;**7**(79).
18. de Amancio GCS, Grabe-Guimarães A, Haikel D, Moreau J, Barcellos NMS, Lacampagne A, et al. Effect of pyridostigmine on in vivo and in vitro respiratory muscle of mdx mice. *Respir Physiol Neurobiol* 2017;**243**:107-14.
19. Cazorla O, Szilagyi S, Vignier N, Salazar G, Kramer E, Vassort G, et al. Length and protein kinase A modulations of myocytes in cardiac myosin binding protein C-deficient mice. *Cardiovasc Res* 2006;**69**:370-80.
20. Farman GP, Tachampa K, Mateja R, Cazorla O, Lacampagne A, Tombe PP. Blebbistatin: use as inhibitor of muscle contraction. *Pflugers Arch - Eur J Physiol* 2008;**455**:995-1005.
21. Schindelin J, Arganda-Carrera I, Frise E, Kaynig V, Longair M, Pietzch T, et al. Fiji — an open source platform for biological image analysis. *Nat Methods* 2012;**9**(7):241.
22. Boulesteix T, Beaurepaire E, Sauviat M-P, Schanne-Klein M-C. Second-harmonic microscopy of unstained living cardiac myocytes: measurements of sarcomere length with 20-nm accuracy. *Opt Lett* 2004;**29**(17):2031-3.
23. Prent N, Green C, Greenhalgh C, Cisek R, Major A, Stewart B, et al. Intermyofilament dynamics of myocytes revealed by second harmonic generation microscopy. *J Biomed Opt* 2008;**13**(4)041318.
24. Recher G, Rouède D, Schaub E, Tiaho F. Skeletal muscle sarcomeric SHG patterns photo-conversion by femtosecond infrared laser. *Biomed Opt Express* 2011;**2**(2):374.
25. Flagg TP, Cazorla O, Remedi MS, Haim TE, Tones MA, Bahinski A, et al. Ca2+-independent alterations in diastolic sarcomere length and relaxation kinetics in a mouse model of lipotoxic diabetic cardiomyopathy. *Circ Res* 2009;**104**(1):95-103.
26. Lopez JR, Kolster J, Zhang R, Adams J. Increased constitutive nitric oxide production by whole body periodic acceleration ameliorates alterations in cardiomyocytes associated with utrophin/dystrophin deficiency. *J Mol Cell Cardiol* 2017;**108**:149-57.
27. Piquereau J, Ventura-Clapier R. Maturation of cardiac energy metabolism during perinatal development. *Front Physiol* 2018;**9**:1-10.
28. Sanger JW, Chowrashi P, Shaner NC, Spalthoff S, Wang J, Freeman NL, et al. Myofibrillogenesis in skeletal muscle cells. *Clin Orthop Relat Res* 2002(403 Suppl):S153-62.
29. Tonino P, Kiss B, Strom J, Methawasin M, Smith JE, Kolb J, et al. The giant protein titin regulates the length of the striated muscle thick filament. *Nat Commun* 2017;**8**(1):1-10.
30. Lahmers S, Wu Y, Call DR, Labeit S, Granzier H. Developmental control of titin isoform expression and passive stiffness in fetal and neonatal myocardium. *Circ Res* 2004;**94**(4):505-13.
31. Amedro P, Vincenti M, De La Villeon G, Lavastre K, Barrea C, Guillaumont S, et al. Speckle-tracking echocardiography in children with Duchenne muscular dystrophy: a prospective multicenter controlled cross-sectional study. *J Am Soc Echocardiogr* 2019;**32**(3):412-22.
32. Cazorla O, Freiburg A, Helmes M, Centner T, McNabb M, Wu Y, et al. Differential expression of cardiac titin isoforms and modulation of cellular stiffness. *Circ Res* 2000;**86**(1):59-67.
33. Meyers TA, Townsend D. Early right ventricular fibrosis and reduction in biventricular cardiac reserve in the dystrophin-deficient mdx heart. *Am J Physiol Heart Circ Physiol* 2015;**308**(4):303-15.
34. Li Y, Zhang S, Zhang X, Li J, Ai X, Zhang L, et al. Blunted cardiac beta-adrenergic response as an early indication of cardiac dysfunction in Duchenne muscular dystrophy. *Cardiovasc Res* 2014;**103**(1):60-71.
35. Saito T, Asai K, Sato S, Hayashi M, Adachi A, Sasaki Y, et al. Autophagic vacuoles in cardiomyocytes of dilated cardiomyopathy with initially decompensated heart failure predict improved prognosis. *Autophagy* 2016;**12**(3):579-87.
36. Williams IA, Allen DG. The role of reactive oxygen species in the hearts of dystrophin-deficient mdx mice. *Am J Physiol - Hear Circ Physiol* 2007;**293**(3):1969-77.
37. Esposito G, Carsana A. Metabolic alterations in cardiomyocytes of patients with Duchenne and Becker muscular dystrophies. *J Clin Med* 2019;**8**:2151.
38. Rubi L, Todt H, Kubista H, Koenig X, Hilber K. Calcium current properties in dystrophin-deficient ventricular cardiomyocytes from aged mdx mice. *Physiol Rep* 2018;**6**(1):1-8.
39. Pioner JM, Guan X, Klaiman JM, Racca AW, Pabon L, Muskheli V, et al. Absence of full-length dystrophin impairs normal maturation and contraction of cardiomyocytes derived from human-induced pluripotent stem cells. *Cardiovasc Res* 2020;**116**(2):368-82, https://doi.org/10.1093/cvr/cvz109.
40. Fanchaouy M, Polakova E, Jung C, Ogrodnik J, Shirokova N, Niggli E. Pathways of abnormal stress-induced Ca2+ influx into dystrophic mdx cardiomyocytes. *Cell Calcium* 2009;**46**(2):114-21.
41. Szibor M, Pöling J, Warnecke H, Kubin T, Braun T. Remodeling and dedifferentiation of adult cardiomyocytes during disease and regeneration. *Cell Mol Life Sci* 2014;**71**(10):1907-16.
42. Bersell K, Arab S, Haring B, Kühn B. Neuregulin1/ErbB4 signaling induces cardiomyocyte proliferation and repair of heart injury. *Cell* 2009;**138**(2):257-70.
43. Kubin T, Pöling J, Kostin S, Gajawada P, Hein S, Rees W, et al. Oncostatin M is a major mediator of cardiomyocyte dedifferentiation and remodeling. *Cell Stem Cell* 2011;**9**(5):420-32.
44. Kyrychenko V, Poláková E, Janicek R, Shirokova N. Mitochondrial dysfunctions during progression of dystrophic cardiomyopathy. *Cell Calcium* 2015;**58**(2):186-95.
45. Kaasik A, Kuum M, Joubert F, Wilding J, Ventura-Clapier R, Veksler V. Mitochondria as a source of mechanical signals in cardiomyocytes. *Cardiovasc Res* 2010;**87**(1):83-91.
46. Youle RJ, Van Der Bliek AM. Mitochondrial fission, fusion, and stress. *Science (80-)* 2012;**337**(6098):1062-5.
47. Ferry A, Messéant J, Parlakian A, Lemaitre M, Roy P, Delacroix C, et al. Desmin is a modifier of dystrophic muscle features in Mdx mice. *bioRxiv* 2019;**32**(0):1-32.
48. Balogh J, Merisckay M, Li Z, Paulin D, Arner A. Hearts from mice lacking desmin have a myopathy with impaired active force generation and unaltered wall compliance. *Cardiovasc Res* 2002;**53**(2):439-50.
49. Garbe CS, Buttgereit A, Schurmann S, Friedrich O. Automated multiscale morphometry of muscle disease from second harmonic generation microscopy using tensor-based image processing. *IEEE Trans Biomed Eng* 2012;**59**(1):39-44.
50. Garcia-Canadilla P, Gonzalez-Tendero A, Iruretagoyena I, Crispi F, Torre I, Amat-Roldan I, et al. Automated cardiac sarcomere analysis from second harmonic generation images. *J Biomed Opt* 2014;**19**(5)056010.